Int. J. Solids Structures Vol. 18, No. 5, pp. 367–380, 1982
Printed in Great Britain.

0020-7683/82/050367-14$03.00/0
Pergamon Press Ltd.

WAVE PROPAGATION IN A RANDOM PARTICULATE COMPOSITE AT LONG AND SHORT WAVELENGTHS

VIKRAM K. KINRA
Department of Mechanical Engineering, University of Colorado, Boulder, CO 80309, U.S.A.

and

ARUN ANAND
IBM Corporation, General Products Division, Tucson, AZ 85744, U.S.A.

(*Received* 27 *August* 1981)

Abstract—This paper is concerned with an experimental determination of the longitudinal and the shear wave velocities, $\langle C_1 \rangle$ and $\langle C_2 \rangle$, in a random particulate composite at both the long and the short wavelength limits. An extensive investigation of the problem has been carried out by using thirty-five specimens with three different ball sizes and five different volume fractions of inclusions. Let $\delta = \lambda/a$, where λ is the shortest of the four wavelengths and a is the inclusion radius. When $\delta \gg 1$, the experiments were found to be in good agreement with the available long-wavelength (or static) analyses; the wave propagation was found to be fairly non-dispersive; and contrary to the key assumption of long-wavelengths, these theories have been shown to be good down to $\delta = 1.15$. When $\delta \approx 1$, the incident time-harmonic sinusoidal toneburst is severely distorted; neither $\langle C_1 \rangle$ nor $\langle C_2 \rangle$ could be measured. When $\delta \ll 1$, the distortion disappears, the wave propagation becomes, once again, weakly dispersive, but $\langle C_1 \rangle$ is significantly higher than its long-wavelength limit.

Finally, some evidence is presented which indicates that the wave-propagation may be occurring along two separate branches: (1) the lower or the acoustical branch; and (2) the upper or the optical branch. These are separated by a cut-off range of frequencies corresponding to $\delta \approx 1$.

1. INTRODUCTION

Considerable advances have been made in the understanding of the mechanics of composite materials in recent years. The man-made composites may be broadly classified into three categories; plate, fibrous, and particulate composites. Whereas the first two have been studied quite extensively, it is only recently that the particulate composites—consisting of particles of one material embedded in the matrix of another—have begun to receive attention. Even here, much of the work has been analytical in nature. A systematic experimental investigation of ultrasonic wave propagation in a *random* particulate composite was reported in [1]. The composite consisted of tiny spheres of glass of mean diameter $2a = 0.3$ mm dispersed in an epoxy matrix; the volume fraction of inclusion, $\tilde{C}$ and the frequency, n, were varied in the range $0.086 < \tilde{C} < 0.533$ and $0.3 < n < 5$ MHz, respectively; *therefore all the data collected belonged to the long-wavelength regime.* The wavespeeds of the longitudinal and shear disturbances, $\langle C_1 \rangle$ and $\langle C_2 \rangle$, respectively, were measured. The principal conclusions of Ref. [1] are:

(1) $\langle C_1 \rangle$, $\langle C_2 \rangle$ data satisfy the *static* bounds due to Hashin and Shtrikman [6], Walpole [7] and Miller [8].

(2) Of the several analyses [3–9] with which the experiments were compared, the identical, independent, dynamic calculations of Datta [3] and Mal and Bose [5] appear to predict the experiments with adequate engineering accuracy for all $\tilde{C}$ and all n tested.

(3) Associated with any frequency n are four wavelengths λ_1, λ_2, λ_1', λ_2' where $(\ )$ and $(\ )'$ denote, respectively, the matrix and the inclusion material, and subscripts $(\ )_1$ and $(\ )_2$ denote, respectively, the longitudinal and shear disturbances. Let $\lambda = \text{MINIMUM}\ (\lambda_1, \lambda_2, \lambda_1', \lambda_2')$ and $\delta = \lambda/a$, where a is the *inclusion radius.* For glass-epoxy combination $\delta = \delta_2$ (see Table 1 for constituent properties). One of the remarkable observations in Ref. [1] is that, in defiance of the underlying assumption of very long-wavelengths common to all the analyses cited [3–9], the agreement between the theories and the experiments remained quite good as δ was *gradually decreased* from very large values (≈ 10) to a fairly small value $\delta = 2.2$. Note that $\delta = 2$ implies that the shortest wavelength equals inclusion diameter. Unfortunately, due to experimental limitations, data at even shorter wavelengths could not be collected.

The objective of this paper is to extend the work reported in Ref. [1] *into the short-wavelength regime.*

The composite studied here is exactly the same as in [1] i.e. glass spheres in TRACAST-3012 epoxy. The principal difference is that in order to probe simultaneously all three regimes of interest ($\delta \gg 1$, $\delta \approx 1$, and $\delta \ll 1$), much larger glass spheres of three different diameters, $2a = 1$ or 2 or 3 mm were used; of course only one size was used in each specimen. In all, thirty-five specimens with the three different ball sizes and five different volume fractions (5, 15, 25, 35 and 45% nominal) were fabricated and tested. $\langle C_1 \rangle$ and $\langle C_2 \rangle$ were measured over the frequency range $0.3 < n < 3.0$ MHz. Following observations are made from this fairly exhaustive study of the problem.

(1) As expected, when $\delta \gg 1$, good agreement between the long-wavelength analysis and the experiments is observed.

(2) As δ is *gradually decreased* the agreement remains quite good until $\delta = 1.15$, i.e. until the shortest wavelength roughly equals the incusion *radius.*

(3) As δ is further decreased a clearly defined transition in the dynamic mechanical behavior of the composite is observed: $\langle C_1 \rangle$ increased suddenly and by large amounts. The transition occurs somewhere in the vicinity of $\delta = 1$.

(4) As δ becomes small compared to unity $\langle C_1 \rangle$ appears to reach a (higher) frequency-independent value.

(5) The wave propagation is shown to occur along two distinct branches: (1) The lower or the acoustical branch; and (2) The upper or the optical branch. These are separated by a cut-off zone, i.e. by a range of frequencies in which $\langle C_1 \rangle$ and $\langle C_2 \rangle$ could not be measured.

(6) Finally, for $\delta < 1$, the comparison between the long-wavelengths analyses and the short-wavelength experiments is shown to become meaningless, as expected; even the bounds are violated. Thus, the need for additional analytical work in the short-wavelength regime is clearly identified.

2. EXPERIMENTAL PROCEDURES

The experimental procedures used in this investigation are similar to the ones reported in Ref. [1]. Therefore, only a brief description is included in the following.

The through-transmission water-immersion ultrasonic tank used in this investigation is shown schematically in Fig. 1. The heart of this apparatus is a pair of accurately matched (in the sense of their frequency response) broad-band piezoelectric transducers. Let $t = 0$ be the instant at which the Time Mark Generator (Tek. TM 184) produces a triggering pulse. The Pulse Generator (Tek PG 501)/Function Generator (Tek. FG 502) combination then generates a toneburst of the desired center-frequency ($0.3 < n < 3.0$ MHz) and duration (10–50 μsec.). The tone-burst is amplified by a radio-frequency Power Amplifier (either E.I.N. 310L or E.I.N. A150) to a peak-to-peak voltage of 40–300 volts and applied to the transmitting transducer. As a

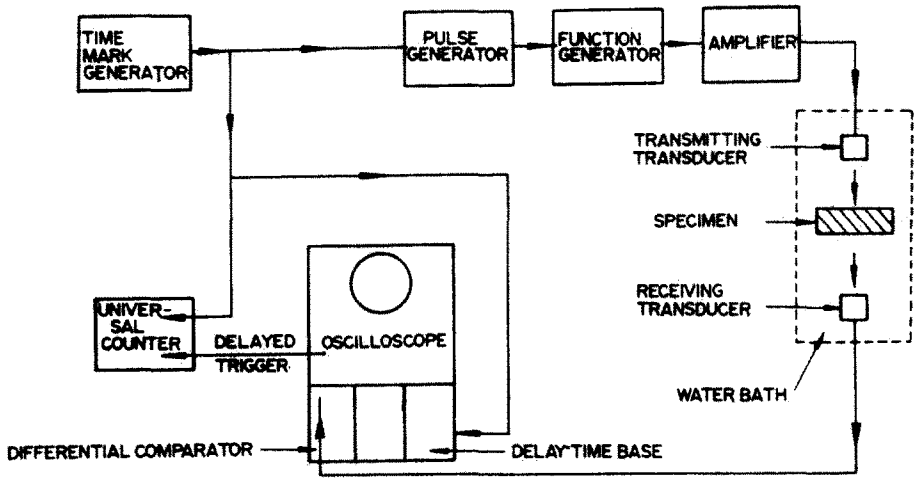

Fig. 1. Schematic of the apparatus.

result, a P-wave is launched in water towards the specimen, the through-transmitted pulse is detected by the receiver and displayed on the lower trace of the oscilloscope (Tek. 7403) whose triggering is delayed by an amount roughly equal to the time-of-flight of the tone-burst between the two transducers; this permits a detailed examination of the received signal. The delay-time is measured accurately with a Universal Counter/Timer (Tek. DC 505A) with an *instrument* accuracy of ± 1 ns. All measurements are made with a *specific peak* near the center of the toneburst where it had reached a steady state; this permits us to assume that the specimen is undergoing steady time-harmonic motion. In most cases, the tone-burst consists of at least twenty cycles; ten on either side of the specific peak.

With the specimen removed, let t_1 and t_2 be respectively the arrival times of the specific peak wehen the transducers are d_1 and d_2 apart. Let t_3 be the arrival time with the specimen in place and the transducers d_2 apart (here the P-wave is normally incident at the specimen); let W be the specimen thickness. Then

$$\langle C_1\rangle^{-1} \equiv \langle S_1\rangle = (t_2 - t_1)/(d_2 - d_1) + (t_3 - t_2)/W, \tag{1}$$

where S implies slowness. Note that the first term on the right is S_w—the slowness of sound in water. When the shear velocity measurements were desired, the specimen was rotated about the vertical axis to an angle, $i > i_{crit}$ where i_{crit} is the angle of incidence beyond which no P-wave is generated in the specimen: By Snell's law $\sin(i_{crit}) = V_w/C_1$, where $V_w = 1/S_w$. Then

$$\langle C_2\rangle = V_w \sin(r)/\sin(i), \tag{2}$$

$$\tan(r) = W \sin(i)/[W\cos(i) - (t_2 - t_3)V_w], \tag{3}$$

where r is the angle of refraction of the shear wave. A systematic error analysis was reported in [1]. The accuracy depends most strongly on W: for the "worst" case, $W \simeq 6$ mm and error $\simeq 1.3\%$; for the "best" case, $W \simeq 24$ mm and error $\simeq 0.5\%$; overall an accuracy of $\pm 1\%$ is claimed in both $\langle C_1\rangle$ and $\langle C_2\rangle$ measurements.

2.1 *Specimen preparation and material description*

The experimental procedures for specimen preparation were—in their essential detail—similar to those described in [1]; their description, therefore, will be omitted here. One exception is that in [1], since particle diameter $2a = 0.3$ mm, a "layer" consisted of four "sub-layers" each containing one sphere. In this work $2a = 1$ or 2 or 3 mm, therefore the sublayers were not necessary and each layer contained exactly one ball in the thickness direction; the layer thickness is given by $d = a(4\pi/3\ \check{C})^{1/3}$. Secondly, an additional precaution was observed in these experiments. Individual layers (before they were stacked and glued together to form the final composite) were subjected to a crude quick visual photoelastic examination under crossed-polaroids; the residual stresses at the sphere-matrix interface were found to be compressive. This is quite consistent with the fact that during the curing process the epoxy undergoes a shrinkage of about 5% whereas shrinkage of glass is relatively little. Thus the assumption of welded-contact in all the analytical works quoted [3–9] is satisfied in our experiments. The constituent properties are listed in Table 1: the epoxy properties [10] were measured in the laboratory; for glass the manufacturer's specifications [11] had to be relied upon because we could not obtain the same chemical composition glass in the form of either a sheet or a rod on which we could make our own ultrasonic measurements. The attenuation α of the matrix (Nepers/mm) was found to be linearly increasing with n: $\alpha = mn$; m is also reported

Table 1. Constituent properties

Material	C_1 (mm/μs)	C_2 (mm/μs)	ρ	m (Nepers/mm-MHz)
TRA-CAST	2.54	1.16	1.180	0.0456
Glass	5.28	3.24	2.492	Negligible

in Table 1. Finally, in order to conduct an extensive experimental investigation of the problem, thirty-five specimens with three different inclusion sizes (1, 2 or 3 mm dia.) and five different volume fractions (5, 15, 25, 35 and 45% nominal) were manufactured and tested; a listing of these specimens is included in Table 2.

3. RESULTS

3.1 *Velocity measurements at long-wavelengths*, $\delta \gg 1$

Although the measurement of $\langle C_1 \rangle$ and $\langle C_2 \rangle$ at long-wavelengths was the province of Ref. [1], these measurements were duplicated in the early stages of this work due to the following considerations. In Ref. [1], $a = 0.15$ mm and the number of layers, l, in the direction of wave propagation was typically 30. Here $a = 1$, 2, or 3 mm and $3 \leq l \leq 16$. Therefore, even though the same constituents were used, there are significant differences in the manner in which the theoretically treated "wave propagation in an unbounded medium" was modelled in Ref. [1] and in this work. It is reassuring to note that after the data are suitably normalized ($\langle C_1 \rangle / C_1$ viewed as a function of $\bar{C}$ and δ) the agreement between the results of [1] and this work is excellent. Secondly, the long-wavelength data was taken as a starting point for extension into the medium- and short-wavelength regimes.

$\langle C_1 \rangle$ data collected at the longest wavelength is presented in Fig. 2; here $\delta_1 = 10.16$, $\delta_2 = 4.64$, $\delta_1' = 21.12$, $\delta_2' = 12.96$, therefore, $\delta = 4.64$. Thus, the long-wavelength assumption is adequately satisfied. Following observations are made: The independently obtained identical bounds due to Hashin and Shtrikman[6] and Walpole[7] for a general two-phase material are satisfied. The somewhat closer bounds, due to Miller[8] in which the "inclusion" is confined to the *shape of a sphere* are also satisfied. Since these are more relevant here, they are shown as solid lines. Note that the bounds[6–8] are *static*. The data are very much closer to the *lower bound* rather than to the upper bound, which is not at all surprising, for as noted by Hashin[12]:

> "... intuitively, for two materials with same volume fractions and same phase modulii, where in the first the stiffer phase is a matrix while in the second the more compliant phase is a matrix, the actual effective modulii of the first material will be closer to the upper bound while those of the second will be closer to the lower bound."

For the case in hand the compliant phase constitutes the matrix. This aspect of Hashin's conjecture concerning the lower bound, has also been verified under a vastly different set of acoustical conditions[2] where the composite consisted of lead spheres in an epoxy matrix so that, in contrast to the glass-epoxy case the inertial mismatch is very high whereas the elastic mismatch is not so large; the measurements, once again, were found to be very much closer to the lower bound, although the spread between the bounds, expectedly, was not as large. Finally, it may be of interest to report here that in experiments now in progress in which extremely thin

Table 2. Glass-tracast specimens

Ball Size / $\bar{C}$ (Nominal)	1 mm Ball				2 mm				3 mm			
	Specimen Number	$\bar{C}$ (Measured)	W	l	Specimen Number	$\bar{C}$ (Measured)	W	l	Specimen Number	$\bar{C}$ (Measured)	W	l
05	1	5.5	13.13	6	19	5.50	17.09	4				
	2	5.35	21.87	10	20	6.02	12.70	3				
	16	5.17	8.69	4								
15	3	15.70	6.07	4	12	16.46	11.96	4	15	15.35	18.08	4
	4	15.70	12.17	8	13	15.81	24.16	8	33	15.54	13.41	3
	5	13.95	7.67	6	25	16.60	12.17	4	35	15.42	36.04	8
					26	16.30	9.02	3				
25					21	25.50	7.59	3	23	25.35	13.32	4
	6	23.87	12.80	10	22	24.85	12.75	5	24	25.66	11.38	3
	7	24.99	19.05	15								
35	8	27.00	5.72	5					31	35.60	10.16	3
	9	26.65	11.43	10					32	35.31	12.95	4
	10	30.35	17.17	15								
45	17	42.03	4.24	4	14	44.08	15.49	7	27	44.71	9.47	3
	18	45.80	6.22	6	29	44.24	8.79	4	28	45.18	12.60	4
	11	42.07	17.37	16	30	43.85	6.60	3	34	45.04	9.40	3

$\bar{C}$ = volume fraction (%), W = specimen width (mm), l = number of layers

elastic spherical shells of glass (*compliant inclusion*) are embedded in a PMMA (stiff) matrix, the measurements are found to be very much closer to the *upper bound*, thus completing an experimental verification of both aspects of the valuable conjecture by Hashin.

Returning to Fig. 2, the experiments agree quite well with the dynamic calculations of Datta[4] for only the dilute suspensions (the theory is claimed correct to $0(\tilde{C})$); with the static calculations of Chen and Acrivos[9] up to moderate concentrations (the theory is claimed correct to $0(\tilde{C}^2)$); and with the independent but identical dynamic calculations of Datta[3], and Mal and Bose[5] up to concentrated suspensions (these theories are claimed correct *at least* to $0(\tilde{C}^2)$).

It is also interesting to note that for the present case of a stiff inclusion the dynamic calculation of [3, 5] *is the same as the static lower bound of* [6, 7]; *for a compliant inclusion the sameness carries over to the upper bound.* Although some additional observations will be made in the sequel, the preceding remarks also apply to the long-wavelength data in Figs. 3–5 where δ is, respectively, 2.32, 1.54 and 1.16.

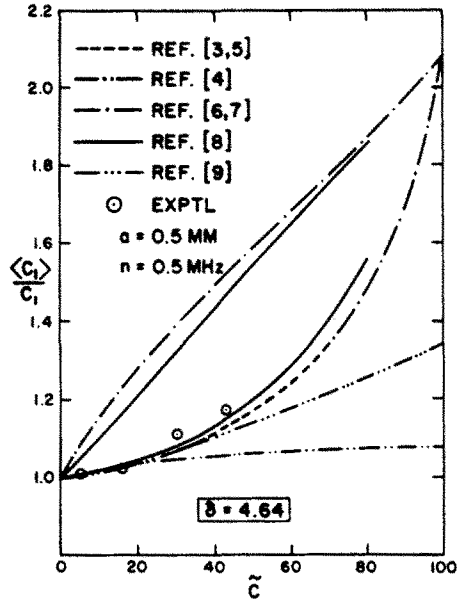

Fig. 2. Longitudinal phase velocity vs volume fraction ($\delta_1 = 10.16$, $\delta_2 = \delta = 4.64$, $\delta_1' = 21.12$, $\delta_2' = 12.96$).

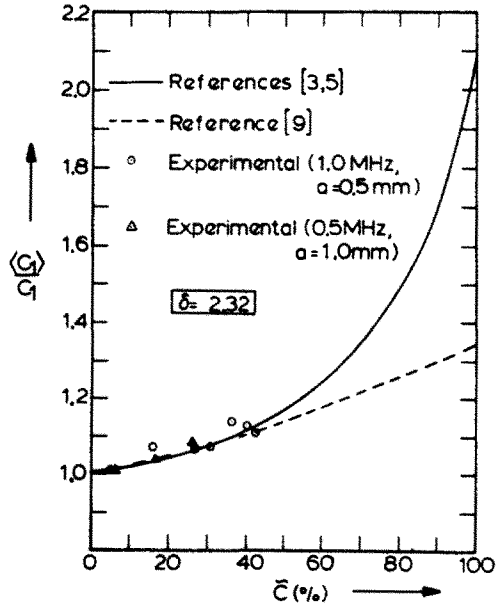

Fig. 3. Longitudinal phase velocity vs volume fraction ($\delta_1 = 5.08$, $\delta_2 = \delta = 2.32$, $\delta_1' = 10.56$, $\delta_2' = 6.48$).

$\langle C_1 \rangle$ data at $\delta = 2.32$ is shown in Fig. 3; here $\delta_1 = 5.08$, δ_2 ($= \delta$) $= 2.32$, $\delta_1' = 10.56$, $\delta_2' = 6.48$. For reasons of corroboration redundant measurements were made; 1 mm dia. balls were tested at 1.0 MHz whereas 2 mm dia. balls were tested at 0.5 MHz. The comparison, within $\pm 1\%$, is considered excellent. With reference to Fig. 4 ($\delta = 1.54$) and Fig. 5 ($\delta = 1.16$) a surprising observation is that the comparison between the theory and the experiment is poorer at the higher $\delta = 1.54$. A plausible conjecture is that $\delta = 1.54$ may be close to one of the resonant frequencies. $\delta = \delta_2 = 1.54$ implies $k_1 a = 1.86$. Reference is now made to the work by Flax and Überall[13] with the emphasis that they considered the case of a *single* inclusion in an unbounded medium. From the numerical results for the case of an iron sphere in aluminum, it is seen that the lowest of the infinitely many resonant frequencies occurs around $k_1 a = 0.5$.

When δ is decreased even further to 1.16 in Fig. 4, the comparison between the theory and the experiment becomes reasonably good again. (The only exception of $\tilde{C} = 45\%$ may be

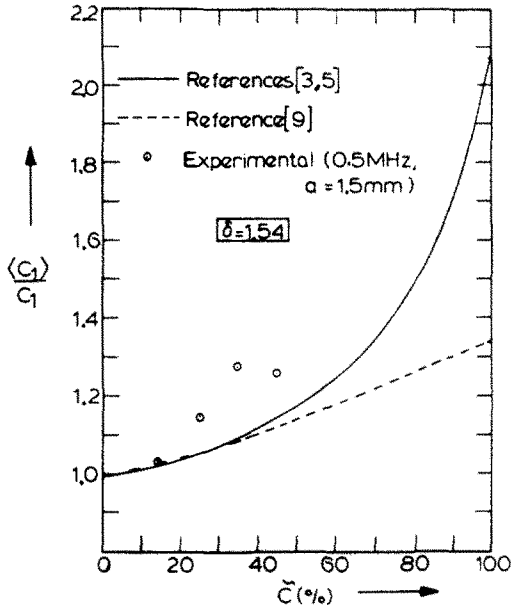

Fig. 4. Longitudinal phase velocity vs volume fraction ($\delta_1 = 3.38$, $\delta_2 = \delta = 1.54$, $\delta_1' = 7.04$, $\delta_2' = 4.32$).

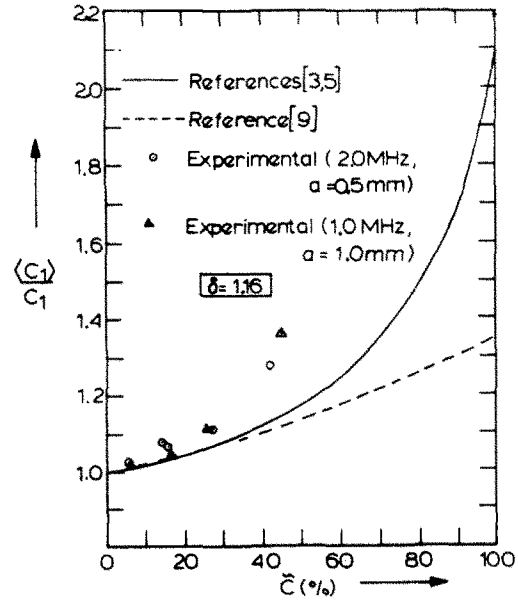

Fig. 5. Longitudinal phase velocity vs volume fraction ($\delta_1 = 2.54$, $\delta_2 = \delta = 1.16$, $\delta_1' = 5.28$, $\delta_2' = 3.24$).

attributed to the fact that here a large fraction of spheres are in direct contact; see Modelling Errors in Appendix 1.) Note that here, again, redundant data were collected: $a = 0.5$ mm at 2.0 MHz and $a = 1.0$ mm at 1.0 MHz.

Shear velocity measurements. In Ref. [1], $\langle C_2 \rangle$ could be measured only for one value of δ, namely $\delta = 8$, primarily for the following reasons: (1) In our method of measuring $\langle C_2 \rangle$, the shear disturbance in the composite is accompanied by a $P \rightarrow S$ and an $S \rightarrow P$ mode conversion with high attendant losses; (2) The scattering cross-section of a sphere, γ, is much higher for incident S-wave as compared to an incident P-wave[17]. Thus, $\langle \alpha_2 \rangle > \langle \alpha_1 \rangle$. (Recall α is attenuation); (3) $\langle \alpha \rangle$ increases as a decreases. (If, for the sake of argument, one neglects the multiple interaction effects, then $\langle \alpha \rangle = (1/2)\ N\ \gamma \pi a^2$, when N is the scatterer density. Since $\tilde{C} = (4/3)\ \pi\ a^3\ N$, $\langle \alpha \rangle = (3/8)\ \gamma \tilde{C}/a$.) Thus, the signal received in [1] for the case of $\langle C_2 \rangle$ was very weak.

By increasing a from 150 μm in [1] to 0.5, 1.0 and 1.5 mm in this work, the attenuation $\langle \alpha_2 \rangle$ decreased sufficiently to permit us to measure $\langle C_2 \rangle$ at three smaller values of δ, namely, 4.64, 2.32 and 1.15; these are shown, respectively, in Figs. 6–8. The remarks concerning the agreement between the long-wavelength theories and the experiments made in the foregoing in connection with $\langle C_1 \rangle$ generally apply to $\langle C_2 \rangle$ as well and will not be repeated. Some additional observations are noted next: (1) For $\delta = 4.64$ (Fig. 2 vs 6) and $\delta = 2.32$ (Fig. 3 vs 7) the $\langle C_1 \rangle$-agreement is much better than the $\langle C_2 \rangle$-agreement. (2) Contrary to expectations the agreement between the theory and the experiment for the case of $\langle C_2 \rangle$ gets monotonically *better* as δ decreases: the comparison may be labelled "excellent" for the smallest $\delta = 1.15$. We are unable to offer any satisfactory explanation for these rather surprising observations. Finally, note that $\langle C_2 \rangle$ is much more sensitive to $\tilde{C}$ than is $\langle C_1 \rangle$.

Before leaving the subject of composite behavior at long wavelengths, a general observation is in order. With collective reference to Figs. 2–8 here and Figs. 3–7 of Ref. [1] it is concluded that the agreement between the experiments and the *long-wavelength analyses*[3, 5–9] may be considered good down to $\delta = 1.15$ ($k_1 a = 2.35$, $k_2 a = 5.37$) or, say, $\delta \simeq 1$; note that this is true across the entire range of volume fractions except, perhaps, at high $\tilde{C}$ and low δ. This observation is quite remarkable, because $\delta = 1$ implies wavelength equals inclusion radius. Thus, these experiments have served another useful purpose in that the range of validity of the long-wavelength theories has been shown to be much wider than had been anticipated on analytical grounds: the theories are claimed to be accurate when $ka \ll 1$, where k is any one of the four wavenumbers k_1, k_2, k_1', k_2'.

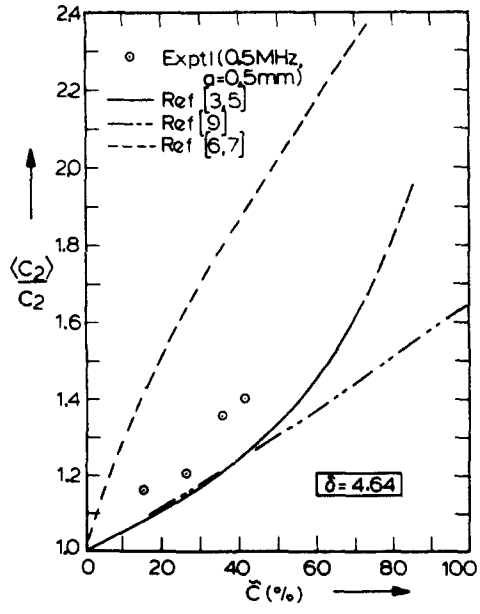

Fig. 6. Shear phase velocity vs volume fraction ($\delta_1 = 10.16$, $\delta_2 = \delta = 4.64$, $\delta_1' = 21.12$, $\delta_2' = 12.96$).

3.2 *Velocity measurements at intermediate wavelengths* $\delta \approx 1$

Efforts to measure $\langle C_1 \rangle$ and $\langle C_2 \rangle$ in the range $0.77 \leq \delta \leq 1.15$ failed. The experimental reasons accompanying the failure are considered both interesting and worth reporting. However, this discussion is deferred to Appendix 2.

3.3 *Velocity measurements at short-wavelengths,* $\delta < 1$

In this section it will be shown that when $\delta < 1$ the comparison between the experimentally measured $\langle C_1 \rangle$ and the predictions of the long-wavelength analyses completely and abruptly breaks down and that the transition occurs somewhere in the vicinity of $\delta = 1$.

$\langle C_1 \rangle$ vs $\bar{C}$ at $\delta = 0.77$, 0.58 and 0.385 are shown collectively in Fig. 9. Firstly, with reference to Figs. 2–5 note that there is a finite positive jump in $\langle C_1 \rangle$ for all $\bar{C}$; this jump is all the more

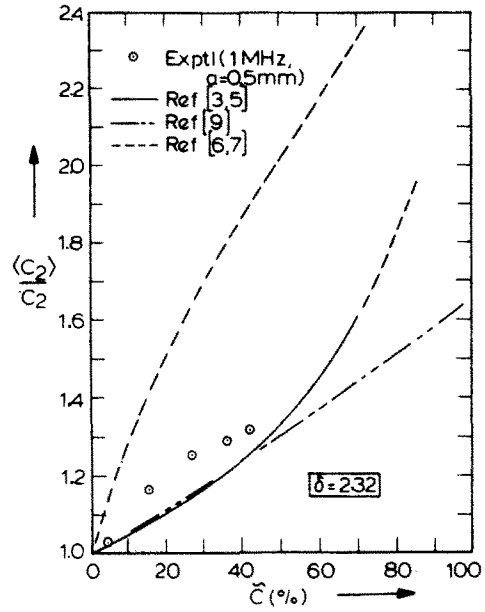

Fig. 7. Shear phase velocity vs volume fraction ($\delta_1 = 5.08$, $\delta_2 = \delta_2 = \delta = 2.32$, $\delta_1' = 10.56$, $\delta_2' = 6.48$).

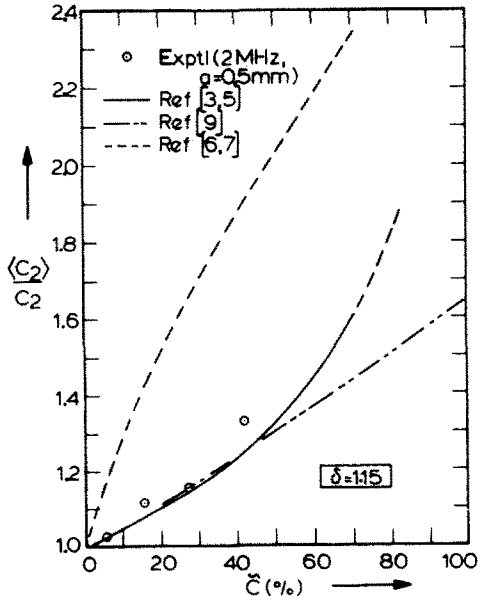

Fig. 8. Shear phase velocity vs volume fraction ($\delta_1 = 2.52$, $\delta_2 = \delta = 1.15$, $\delta_1' = 5.23$, $\delta_2' = 3.21$).

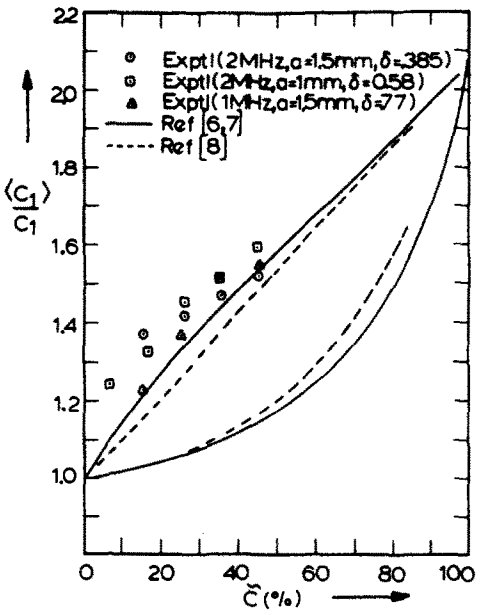

Fig. 9. When wavelength is small compared to the inclusion radius the longitudinal velocity violates the static bounds.

surprising at low $\bar{C} = 5\%$. The increase is of the order of 20–40% (see 1% measurement error). Secondly, $\langle C_1 \rangle$ appears to be a linear function of $\bar{C}$ for all three δ. However, it is believed that this apparent linearity is a mere coincidence for the following simple reason: As $\bar{C} \to 0$, $\langle C_1 \rangle / C_1$ must $\to 1.0$; as $\bar{C} \to 1.0$, $\langle C_1 \rangle / C_1$ must $\to C_1'/C_1 = 2.08$, regardless of δ. The bounds [6–8] are also shown in this figure, more for contrast than for comparison. (Recall that calculations of [3, 5] are the same as the lower bound of [6, 7].) The measurements, which used to cluster around the lower bound for $\delta \gg 1$, have now exceeded the upper bound. Clearly, the long-wavelength analyses are not at all applicable when $\delta < 1$. Finally, it appears that as $\delta \to 0$ (very high frequencies) $\langle C_1 \rangle$ approaches a constant value; this is explored further in Section 3.4.

3.4 *Frequency—wavenumber relationship*

Moon and Mow[14] considered wave propagation, at long-wavelengths, in a ***random homogeneous rigid-particulate composite*** under the following key assumptions: (1) Inclusions are very heavy, i.e. $\rho'/\rho \gg 1$; (2) Suspension is dilute, $\bar{C} \ll 1$, i.e. multiple interaction effects are completely ignored. Clearly, the present experiments do not conform to the key assumptions of the theory: a quantitative comparison was, in fact, found to be extremely poor. However, there is one aspect of Moon and Mow's work which is of interest here. They postulated the existence of two distinct branches along which wave propagation can occur; these are the familiar acoustical (or lower) branch and the optical (or upper) branch separated by a cut-off frequency, Ω_c, see Fig. 2 of Ref. [14]. Ω_c represents the natural oscillatory frequency of the spherical particles in their elastic surroundings. In other words, Ω_c is due to ***individual particle dynamics.*** At the risk of stating the obvious, we emphasize that this (single) Ω_c in a ***random*** composite should be distinguished from the (infinitely many) cut-off frequencies in a ***periodic*** composite. The latter are due to destructive interference of the waves scattered by the particles located in a periodic structure. In other words, these are due to ***lattice dynamics.*** In the following, we present some evidence which suggests that the wave propagation in our experiments may, in fact, be occurring along these two branches.

We introduce a dimensionless frequency, Ω, and a dimensionless wavenumber, ξ, by:

$$\Omega = 2\pi n a / C_1 = k_1 a \quad \text{and} \quad \xi = \langle k_1 \rangle a, \tag{4}$$

then $\Omega/\xi = \langle C_1 \rangle / C_1 = \beta$(say). Ω vs ξ for various $\bar{C}$ are shown in Fig. 10. Note that only $\bar{C} = 5\%$ is shown correctly to scale on the right. For clarity, the remaining $\bar{C}$ curves have

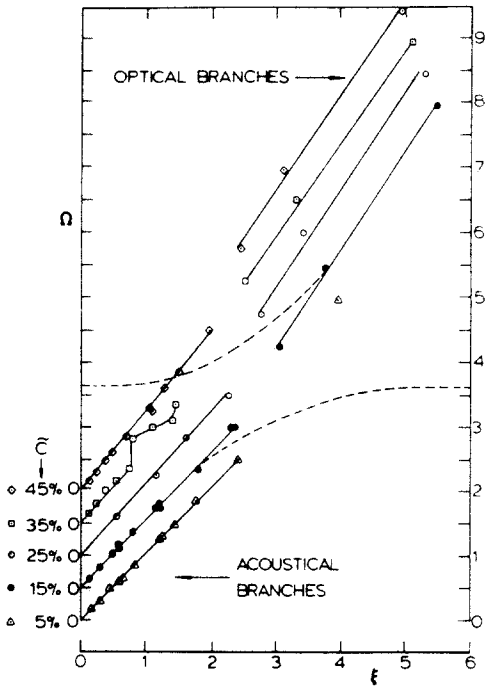

Fig. 10. Ω vs ξ plots reveal the acoustical and the optical branches. Hypothetical lines of extension when the radiation damping is absent (- - - -) and when it is present (. . . .). Only $\tilde{C} = 5\%$ shown correctly to scale on the right. Remaining $\tilde{C}$ shifted by 0.5 on the Ω-scale.

each been shifted by 0.5 on the Ω-scale; no shifting has been done on the ξ-scale. $\Omega = 0$ for each $\tilde{C}$ is indicated on the left. Attention is first drawn to the case $\tilde{C} = 15\%$. Even though it may not appear to be so, the slopes of the two branches are significantly different: As $\Omega \to 0$, $\beta = 1.02$ (lower branch); at $\Omega = 7.46$, $\beta = 1.36$ (upper branch). Following Moon and Mow, Fig. 2 of Ref. [14], the broken lines are hypothetical extensions of the two branches for the case when radiation damping is absent. As it is, the radiation damping is quite strong in our experiments due to the high volume fraction and the multiple interaction effects; the dotted line is the corresponding hypothetical extension. In order to bring out more clearly the frequency dependence of velocity, β is plotted vs Ω in Fig. 11.† Attention is now drawn to the corresponding curve ($\tilde{C} = 15\%$) in Fig. 11. When $\Omega < 2.5$ the wave propagation is weakly dispersive. The range $2.5 < \Omega < 3.75$ is labelled as the "forbidden zone" in the sense that $\langle C_1 \rangle$ could not be measured due to severe harmonic distortion. When $\Omega > 3.75$, where $\langle C_1 \rangle$ measurements could be resumed, β takes a large positive jump (over its value for small Ω), wave propagation becomes, once again, weakly dispersive, and β appears to reach a frequency-independent value at high frequencies.

Admittedly, the evidence is not sufficiently convincing to permit one to state unequivocally that the wave propagation is occuring along the two separate branches postulated by Moon and Mow. Nevertheless, it is clear that there are significant differences in the behavior of the composite in going from the low-frequency regime ($\Omega < 2.5$) to the high frequency regime ($\Omega > 3.75$). To the extent that the approximate theory of Moon and Mow (rigid particles, dilute concentration) is applicable to the present experiments, we are led to conjecture that, in Fig. 10, the lower curve is the acoustical branch and the upper curve is the optical branch.

Essentially the same remarks apply to the $\tilde{C} = 5\%$ curve in Fig. 10 and 11. However, for $\tilde{C} \geq 25\%$ curves, the wave propagation in the low-frequency regime becomes increasingly more

†(1) Only $\tilde{C} = 5\%$ is drawn correctly to scale on the right. For clarity, the remaining $\tilde{C}$-curves are shifted by 1.0 on the β-scale. There is no shifting on the Ω-scale, however. (2) Whenever two values of β are plotted against the same Ω, it implies that two different specimens were used. The difference is, generally, more due to modelling errors than the measurement errors. (3) Additional data for $\tilde{C} = 5\%$ for large Ω could not be collected due to harmonic distortion. (4) data from Ref. [1] has been used to supplement the data collected in this work. (5) The values of β at $\Omega = 0$ are calculated from Ref. [4–6].

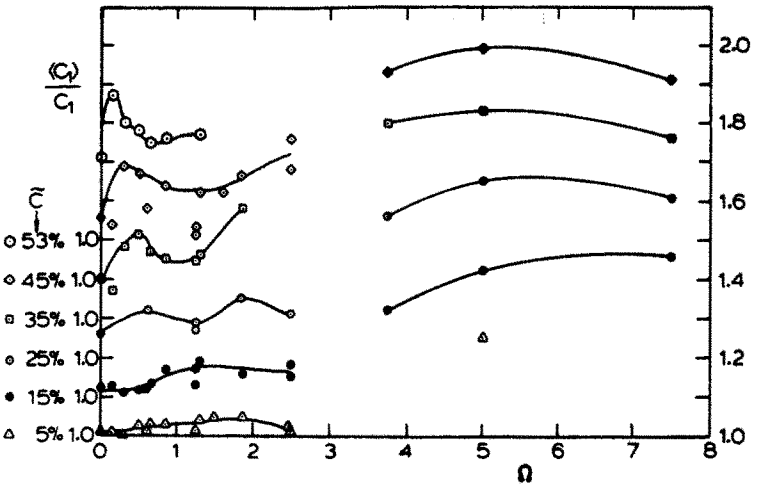

Fig. 11. Longitudinal phase velocity vs. normalized frequency. Only $\tilde{C} = 5\%$ shown correctly to scale on the right. Remaining $\tilde{C}$ shifted by 1.0 on the β-scale.

dispersive as $\tilde{C}$ is increased. The following is offered as a plausible explanation. Flax and Überall[13] have studied the resonant scattering of elastic waves from a spherical elastic inclusion in an unbounded medium. They showed that there is a doubly-infinite series of resonant frequencies and that for the case of an iron sphere in an aluminum matrix, the *smallest* of these occurs at about $k_1 a = 0.5$. We conjecture that the particle resonance is responsible for the dispersion along the acoustical branch. It follows that the observed dispersion should increase with $\tilde{C}$ (more balls); this is borne out by the experiments.

Attention is now turned to the "forbidden zone", $2.5 < \Omega < 3.75$. Following plausible scenario is offered as an explanation for failure to measure wave velocities (see also Appendix 2). In this range, the wave propagation is controlled by the particle resonances. Since the resonant frequencies are closely spaced (see Fig. 4 of Ref. [13] and also Appendix H of Ref. [15]), for any excitation or tone-burst frequency n in this range, there will be one or more resonant frequencies in the neighborhood. Since, a tone-burst is never a pure monochromatic wave, these resonant modes will be excited; also the scattering cross-section of a particle becomes large at or near its natural frequency. The received signal will be a superposition of the incident frequency and the excited resonant frequencies. This may very well be the reason for the observed harmonic distortion (see Fig. A1). This conjectured scenario is also consistent with another observation. Since this range was carefully probed with small increments in Ω, the amplitude of the received signal (the central portion away from the transients at the head and the tail of the toneburst) was seen to undergo large (order of magnitude) and rapid fluctuations with Ω. This may be happening because when n coincides with one of the dominant resonant modes, the scattering cross-section (and hence the composite attenuation $\langle\alpha\rangle$) becomes very large. The fact that when this phenomenon was observed the *transients* at the two ends of the toneburst were observed to be relatively very, very large (by one or two orders ofmagnitude) lends further credibility to this conjecture.

Finally, the numerical values of all the data presented in this work may be found in Appendix 3.

4. CONCLUSIONS

Ultrasonic wave propagation in a random particulate composite has been studied extensively in both the long and short wavelength limits. Thirty-five specimens with three different ball sizes and five different volume fractions were used. The phase velocities of the longitudinal ($\langle C_1 \rangle$) and the shear ($\langle C_2 \rangle$) waves were measured. In the long-wavelength limit ($\delta \gg 1$) the wave propagation is fairly non-dispersive and the experiments agree quite well with the available long-wavelength (or static) theories. In defiance of the key assumption of long wavelengths (infinite wavelengths for the static cases) these theories have been shown to be good down to $\delta = 1.15$. At the intermediate wavelengths, $\delta \approx 1$, the incident wave suffers from severe

harmonic distorsion; neither $\langle C_1 \rangle$ nor $\langle C_2 \rangle$ could be measured. When $\delta < 0.77$, the distortion disappears, the wave propagation becomes, once again, weakly dispersive, and $\langle C_1 \rangle$ is significantly and consistently higher than its long-wavelength limit.

When the velocity data is recast in the form of a dimensionless frequency vs a dimensionless wavenumber, it reveals what appear to be two distinct branches of wave propagation: (1) the lower or the acoustical branch, and (2) the upper or the optical branch.

Acknowledgements—Thanks are due to Karl Rupp for his help in designing, and fabricating the ultrasonic apparatus. Thanks are also due to Karl Rupp and Rich Cowgill for their continued technical assistance through the course of this investigation, and to Marie Hornbostel for her immense patience and care in preparing this manuscript.

The financial support of the National Science Foundation under grant ENG 78-10168 to the University of Colorado, Boulder, is gratefully acknowledged.

REFERENCES

1. V. K. Kinra, M. S. Petraitis and S. K. Datta, Ultrasonic wave propagation in a random particulate composite. *Int. J. Solids Structures* **16**, 301–312 (1980).
2. V. K. Kinra and S. K. Datta, Wave propagation in a lead-epoxy random particulate composite. To be published.
3. S. K. Datta, Scattering by a Random Distribution of Inclusions and Effective Elastic Properties: Continuum Model of Discrete Systems (Edited by J. W. Provan), pp. 111–127. University of Waterloo Press (1978).
4. S. K. Datta, A self-consistent approach to multiple scattering by elastic ellipsodial inclusions. *J. Appl. Mech.* **44**, 657–662 (1977).
5. A. K. Mal and S. K. Bose, Dynamic elastic moduli of a suspension of imperfectly bonded spheres. *Proc. Cambridge Philosophical Soc.* **76**, 587–600 (1974).
6. Z. Hashin and S. Shtrikman, A variational approach to the theory of the elastic behavior of multiphase materials. *J. Mech. Phys. Solids* **11**, 127 (1963).
7. L. J. Walpole, On bounds for the overall elastic moduli of homogeneous systems. *Int. J. Mech. Phys. Solids* **14**, 151 (1966).
8. M. N. Miller, Bounds for effective bulk modulus of heterogeneous materials. *J. Math. Phys.* **10**, 2005 (1969).
9. H. S. Chen and A. Acrivos, The effective elastic moduli of composite materials containing spherical inclusions at non-dilute concentrations. *Int. J. Solids Structures* **14**, 349–364 (1978).
10. TRA-CAST 3012. Manufactured by TRA-CON, Inc., Resin Systems Division, 55 North Street, Medford, Mass. 02155, (617) 391–5540. It is a low viscosity 100% solids (no solvents) epoxy resin and hardener system. Mixing proportions: 46 parts hardener, 100 parts resin. After mixing, the solution was placed in a vacuum chamber until all air was evacuated. The epoxy was then cured for 24 hr at 65°C.
11. Glass spheres 1, 2 and 3 mm were obtained from Sargent Welch Scientific, P.O. Box 7196, Denver, Colorado 80207, (303) 399–8220.
12. Z. Hashin, Theory of composite materials. *Mechanics of Composite Materials, Proc. 5th Symp. on Naval Structural Mech.* Philadelphia, 201–242 (1967).
13. L. Flax and H. Überall, Resonant Scattering of elastic waves from spherical solid inclusions. *J. Acous. Soc. Am.* **67**, 1432–1442 (1980).
14. F. C. Moon and C. C. Mow, Wave propagation in a composite material containing dispersed rigid spherical inclusions, Rand Corporation Report RM-6139-PR, Rand, Santa Monica, California, (1970).
15. R. Truell, C. Elbaum and B. B. Chick, *Ultrasonic Methods in Solid State Physics.* Academic Press, New York (1969).

APPENDIX 1

(1) *Modelling errors*

In addition to the errors of measurement ($\pm 1\%$ in $\langle C_1 \rangle$ and $\langle C_2 \rangle$) there are modelling errors present. These are: (1) In spite of all the precautions, direct contact between a small fraction of spheres could not be avoided. The theories cited in this work assume no direct contact. Heuristically, one would expect this source to cause measured $\langle C_1 \rangle$ to be somewhat *higher* than the calculated $\langle C_1 \rangle$ particularly at high volume fractions. This is borne out by the experiments; (2) The theories treat unbounded media; the specimens have a finite number of layers in the direction of wave propagation. In the experiments when the *P*-wave in water strikes the specimen, the refracted wave must interact with a certain number of layers before the theoretically assumed effective plane wave is fully established. This phenomenon is often referred to as the *boundary layer effect.* A *direct* measurement of this effect is beyond the scope of this work. Nevertheless, wherever possible experiments were carried out to estimate the effect of the boundary layer on the measured quantities. These are described in Section 2 below. (3) Finally, we had to assume, of necessity, that when a plane wave in water strikes the specimen boundary, the refracted *P*- and *S*- waves are also plane.

(2) *The Boundary layer effect*

For the case of 1 mm spheres, three specimens were prepared for each $\hat{C}$, except 25%, see Table 2. The three independent measurements of velocity were found to agree within 1%. (Occasionally, the errors were higher, but these may be attributed to the fact that the precise (measured) $\hat{C}$ is never exactly the same for two specimens of same nominal $\hat{C}$.) Therefore, the boundary layer effect is negligibly small for the 1 mm sphere specimens. A corollary is that $l = 3$ serves as an empirical upper bound on the boundary layer thickness (BLT) (note $l_{\min} = 4$). Now, in principle, a closer upper bound on BLT can be placed by conducting similar experiments on successively thinner specimens, i.e. $l \leq 3$. In practice, this could not be done for the following reasons. In the present method of measurement, in addition to the Through-Transmitted-Pulse (TPP), the receiver also detects a sequence of TIRPS's (Twice Internally Relected Pulses) at a time interval of $2W/\langle C_1 \rangle$. The following data-rejection criterion was used throughout this work: If the TTP had not reached steady state prior to the arrival of the first TIRP, the data was rejected. It is for these reasons that velocity could not be measured with 1 mm sphere specimens fof $l < 4$. Finally, since l varied from 4 to 16 (for 1 mm sphere specimens), boundary layer effect was never a problem.

In the early stages of this work, 2 mm and 3 mm specimens were also fabricated with a large l ($l \approx 10$). With the exception of very low frequencies, satisfactory measurements could not be made because of very low received signals (sometimes less than 1 millivolt) due to the following reasons. Thickness of a layer is given by $d = a\,(4\pi/3\bar{C})^{1/3}$ i.e., d is proportional to a. $W = ld$. Total attenuation is $e^{-\langle\alpha\rangle W}$. Therefore, for 2 and 3 mm specimens the bulk of the data was collected with undesirably thin specimens of $l = 3$ and $l = 4$. Following precautions were taken to ensure against the errors due to the boundary layer effect: (1) Two independent velocity measurements were made for each $\bar{C}$; the data was generally found to agree within 1%. Note that TIRP is longer a problem here due to increased W. (2) Specimen preparation is a very time consuming process. Therefore, as much as possible it was desirable to use the same specimen across the entire frequency range ($\langle\alpha\rangle$ increases almost linearly with n, see Ref. [1]); hence, small l. But, occasionally, *for the purpose of calibration* thicker 2 mm and 3 mm specimens were also made, see specimen 13 ($l = 8$), 14 ($l = 7$) and 35 ($l = 8$) in Table 2. Together with the 3- and 4- layer specimens of the same $\bar{C}$, these calibration specimens were tested only at low frequencies. It was reassuring to note that the velocity measurements agreed, once again within 1%.

Admittedly, we have been unable to measure directly the error (if any) produced by the ubiquitous boundary layer. Nevertheless, from the numerous precautionary and redundent measurements discussed in the foregoing we are led to conclude that this error is small and may be subsumed in the 1% error of measurement.

APPENDIX 2

Experimental reasons for failure of $\langle C_1\rangle$ and $\langle C_2\rangle$ measurements at intermediate wavelengths, $\delta \approx 1$.

As described in the Experimental Procedures all measurements are made with a specific peak in the incident signal received through water. The *same peak* is later identified in the toneburst received through the specimen. Whenever an unequivocal one-to-one correspondence between the peaks of the signals is not possible, data is rejected.

For $\delta \gg 1$ this correspondence was never a problem: a typical signal through a specimen for $\delta = 1.54$ is shown in Fig. A1(a). The corresponding through-the-water signal looks very much alike and is not shown. As δ is gradually decreased below 1.15 an additional peak is seen to emerge. This peak begins to take a more and more definite shape as δ is further decreased. At the same time the entire waveform undergoes a gradually increasing distortion. At $\delta = 0.96$ the state of affairs may be seen in Fig. A1(b). Note, in particular, the *additional peak* around the 2 cm. location. Since a peak can be located only relative to the head of the pulse the unequivocal correspondence mentioned earlier cannot be established here; therefore, data was not collected. As δ is further decreased, the peak "marches forward" towards the head of the pulse while simultaneously moving up and down the waveform. Finally, around $\delta = 0.8$ the additional peak clears the head of the toneburst: at $\delta = 0.325$ the received signal is shown in Fig. A1(c). The important point here is that even in the presence of this "fore-runner wave", an "unequivocal correspondence" could be established and the process of data collection resumed: reducing the duration of the toneburst down to *only one full cycle* was taken as a starting point for this operation.

Shear wave measurements

Unlike $\langle C_1\rangle$, $\langle C_2\rangle$ could not be measured for any $\delta < 1.15$. In addition to the waveform distortion, $\langle C_2\rangle$ measurements suffer from another problem. When $\delta \gg 1$, $\langle C_1\rangle$ is measured first and then the critical angle of incidence beyond which

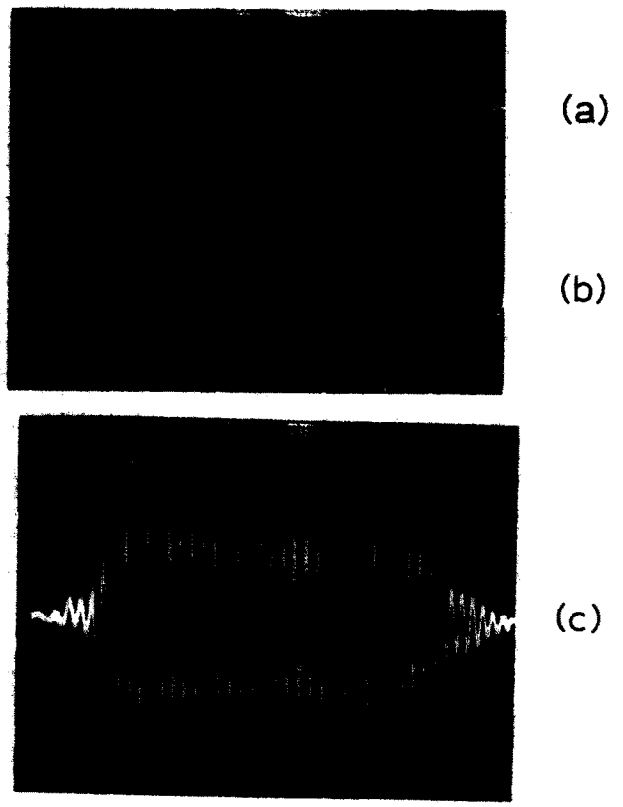

Fig. A1. Signal received with a specimen with $a = 1.5$ mm, $\bar{C} = 25.4\%$, and (a) $\delta = 1.54$ ($\Omega = 1.86$), (b) $\delta = 0.96$ ($\Omega = 2.99$), and (c) $\delta = 0.325$ ($\Omega = 8.84$).

P-wave is not generated in the composite is calculated by the Snell's law: $i_{crit} = \mathrm{Sin}^{-1}(Vw/\langle C_1 \rangle)$. Then $\langle C_2 \rangle$ is measured at some $i > i_{crit}$. The Snell's law was found to be satisfied when $\delta \gg 1$. On the other hand for $\delta < 1.15$ the Snell's law was found to be violated in the following sense. Figure A2(a) shows incident signal through water; the tone-burst has been purposely shrunk to only two cycles to preserve clarity. The calculated i_{crit} for this particular situation is 31°. For $i = 37° > i_{crit}$ the received signal is shown in Fig. A2(b). The two received signals correspond, sequentially, to the refracted P- and S-wave. Had δ been $\gg 1$, P-wave would have completely disappeared. As it is its amplitude is roughly the same as that of the shear wave, thus disallowing $\langle C_2 \rangle$ measurements with a toneburst of 10 or 20 cycles. Note that one could go ahead and measure $\langle C_2 \rangle$ with a 2-cycle toneburst. However, it is very difficult to judge how badly the assumption of steady time harmonic motion of the specimen is violated in that case and, therefore, data collection was not carried out.

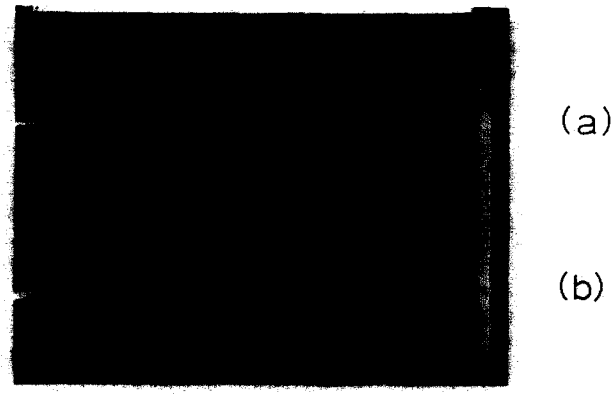

Fig. A2. Violation of Snell's Law, (a) Signal received through water, (b) P- and S-waves received through the specimen for an angle of incidence $i = 37°$ which is greater than $i_{crit} = 31°$.

APPENDIX 3. NUMERICAL VALUES OF DATA

$\bar{C}$ = 5%

Ω	β	ξ	a, mm
.62	1.01	.61	0.5
1.24	1.01	1.22	0.5
1.24	1.01	1.22	1.0
1.87	1.03	1.81	1.5
2.48	1.02	2.42	0.5
2.48	1.01	2.45	1.0
4.95	1.25	3.96	1.0
From [1]			
.15	1.01	.15	0.15
.30	1.01	.30	0.15
.50	1.03	.47	0.15
.65	1.03	.63	0.15
.85	1.03	.83	0.15
1.30	1.04	1.25	0.15
1.50	1.05	1.43	0.15
1.85	1.05	1.76	0.15

$\bar{C}$ = 35%

Ω	β	ξ	a, mm
1.24	1.14	1.08	0.5
1.87	1.28	1.46	1.5
3.73	1.50	2.48	1.5
4.95	1.53	3.23	1.0
7.46	1.46	5.10	1.5
From [1]			
.15	1.07	.14	0.15
.30	1.18	.25	0.15
.50	1.21	.41	0.15
.65	1.17	.56	0.15
.85	1.15	.74	0.15
1.30	1.16	.81	0.15
1.60	1.15	1.39	0.15

$\bar{C}$ = 15%

Ω	β	ξ	a, mm
.62	1.02	.61	0.5
1.24	1.07	1.16	0.5
1.24	1.07	1.16	0.5
1.24	1.04	1.19	1.0
2.48	1.08	2.29	0.5
2.48	1.07	2.31	0.5
2.48	1.05	2.36	1.0
3.73	1.22	3.05	1.5
4.95	1.32	3.75	1.0
7.46	1.36	5.48	1.5

$\bar{C}$ = 45%

Ω	β	ξ	a, mm
.62	1.18	.52	0.5
1.24	1.13	1.09	0.5
1.24	1.11	1.11	0.5
1.87	1.26	1.48	1.5
2.48	1.28	1.93	0.5
2.48	1.36	1.82	1.0
3.73	1.53	2.44	1.5
4.95	1.59	3.11	1.0
7.46	1.51	4.94	1.5
From [1]			
.15	1.14	.13	0.15
.30	1.29	.23	0.15
.50	1.27	.39	0.15
.85	1.24	.69	0.15
1.30	1.22	1.07	0.15
1.60	1.22	1.31	0.15

$\bar{C}$ = 25%

Ω	β	ξ	a, mm
.62	1.12	.55	0.5
1.24	1.07	1.16	0.5
1.24	1.09	1.14	1.0
1.87	1.15	1.62	1.5
2.48	1.11	2.23	0.5
2.48	1.11	2.23	1.0
3.73	1.36	2.74	1.5
4.95	1.45	3.42	1.0
7.46	1.41	5.29	1.5

$\bar{C}$ = 53%, Ref. [1]

Ω	β	ξ	a, mm
.15	1.37	.11	0.15
.30	1.30	.23	0.15
.50	1.28	.39	0.15
.65	1.25	.52	0.15
.85	1.26	.67	0.15
1.30	1.27	1.02	0.15

$\langle C_2 \rangle / C_2$, a = 0.5 mm

$\bar{C}$ ↓ Ω →	0.62	1.24	2.48
5	-	1.03	1.03
15	1.16	1.16	1.12
25	1.21	1.26	1.16
35	1.36	1.29	-
45	1.41	1.32	1.34